6th European Conference on Computational Mechanics (ECCM 6)
7th European Conference on Computational Fluid Dynamics (ECFD 7)
1115 June 2018, Glasgow, UK

# AN IMMERSED BOUNDARY METHOD WITH DIVERGENCE-FREE INTERPOLATION FOR UNSTRUCTURED POLYHEDRAL GRIDS

**DUARTE M. S. ALBUQUERQUE[1], DIOGO M. C. MARTINS AND JOSÉ C. F. PEREIRA**

LAETA, IDMEC, Instituto Superior Técnico, Universidade de Lisboa
1 - DuarteAlbuquerque@tecnico.ulisboa.pt

**Key words:** Immersed Boundary Method, Spurious Force Oscillations, Moving Body Problems, Unstructured Polyhedral Grids, Continuity Constrainted Least-Squares (CCLS).

**Abstract.** A new immersed boundary interpolation method for discrete forcing methods is presented. It decreases the spurious force oscillations (SFO) in the pressure field and consequently in the body force calculations, which is a common issue in several immersed boundary methods. The method applies a divergence-free constraint directly in the velocity interpolation. It also guarantees a field continuity between each adjacent interpolation polynomial. This approach strictly enforces a divergence-free velocity field in the reconstruction domain, reducing the time discontinuities caused by the applied boundary conditions near the solid boundary.

Due to its flexibility, the current method can be applied with any arbitrary unstructured grid. Several tests are carried out to validate the technique with different grid types: polyhedral, triangular and Cartesian. The method is shown to compute the correct velocity and pressure fields independently of the grid type. The effects of the cell topology in the SFO are studied and the polyhedral grids are proven to be superior to their Cartesian and triangular counterparts.

Finally, some examples of moving bodies are provided, in a computational domain with complex static boundaries. The new method allows the use of unstructured grids for the outer fixed boundaries, providing good geometry conformance and therefore good flow resolution.

## 1 Finite Volume Discretization in Unstructured Grids

The numerical methods of the bulk flow solver used have been previously verified in several flow conditions [1, 2]. Additionally, detailed descriptions of the implemented methods can be found in the PhD Thesis from Magalhães [3] and Albuquerque [4].

In a finite volume numerical approach, the Navier-Stokes equations of the incompressible flow are transformed in their integral form, where the Gauss theorem can be applied to the convective and diffusive terms. After this treatment, the momentum equations are

written as:

$$\underbrace{\int_{\Omega} \frac{\partial \mathbf{u}}{\partial t} dV}_{\text{temporal term}} + \underbrace{\int_{\partial\Omega} \mathbf{u}\mathbf{u}.d\mathbf{S}}_{\text{convective term}} = \underbrace{\int_{\partial\Omega} \nu \nabla \mathbf{u}.d\mathbf{S}}_{\text{diffusive term}} + \underbrace{\int_{\Omega} -\frac{1}{\rho} \nabla p \, dV}_{\text{pressure term}} \tag{1}$$

each of the terms in equation (1) is treated using a specific numerical scheme for unstructured grids. To solve the coupling between momentum and continuity equations, segregated algorithms have been developed, such as the SIMPLE [5] and the PISO [6] ones. A detailed explanation of these two algorithms is done in the following works [4, 7], respectively.

In the case of unstructured grids, the numerical schemes must have additional correction terms that consider the local grid quality of the mesh, which can be measured using concepts such as warp angle, also called skewness, non-orthogonality angle and volume ratio which were described by Juretic [8].

Skewness, also known as eccentricity by some authors, refers to the distance between a face centroid and the intersection of the face $f$ and the distance vector $\mathbf{d}$, this latter one unities the two adjacent cells $P_0$ and $P_1$. Unless the interpolation considers the face's centroid, the method will not achieve second order accuracy due to the Gauss-Legendre quadrature's violation of the integral convective term. For this reason, skewness corrections exist and solvers can achieve the desired second order accuracy even in low grid quality meshes.

Warp or non-orthogonality angle, refers to the angle between the face's normal and the distance vector $\mathbf{d}$. In a diffusive scheme, the simple finite difference computes the dependent variable's first derivative at a face's centroid, however this method yields inaccurate results when this angle is higher than zero. Both the warp angle and the skewness can be visualized in figure 1.

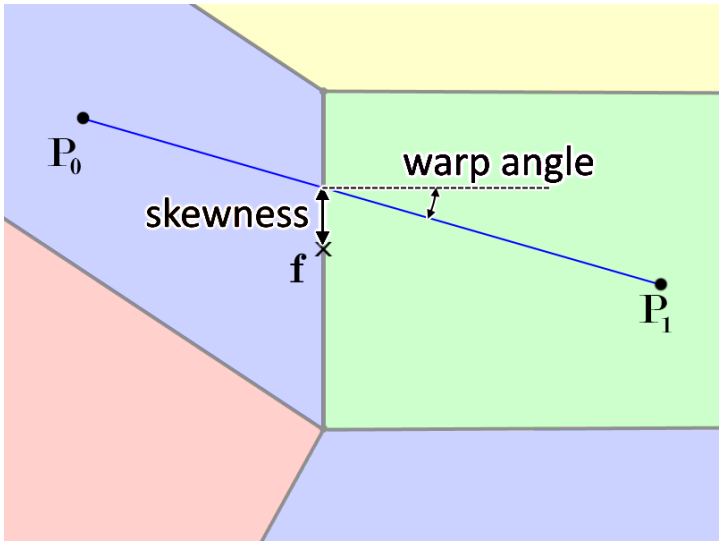


**Figure 1**: Geometric representation of the skewness and the warp angle grid quality metrics.

The convective scheme computes the face value $\phi_f$ of the dependent variable $\phi$ and it is sensitive to the grid skewness. To address this issue, a special interpolation blending factor $\eta_{TRI}$ and a skewness correction term proposed by Juretic [8] are considered. The resulting convective scheme is expressed by:

$$\phi_f = \eta_{TRI}\phi_{P_0} + (1-\eta_{TRI})\phi_{P_1} + \underbrace{(\mathbf{f}-\mathbf{P_0}-\eta_{TRI}\mathbf{d}).(\overline{\nabla\phi})_f}_{\textbf{skewness correction}} \tag{2}$$

where $\mathbf{f}$ is the coordinates vector of the face's centroid. The term identified as skewness correction makes use of the averaged cell centered gradients of the adjacent cells, $\overline{\nabla\phi}$. With this correction term, the convection scheme becomes second order accurate for most unstructured grids.

The blending factor $\eta_{TRI}$ corresponds to an interpolation to the point that is geometrically closer to $\mathbf{f}$ at the line defined by $\mathbf{d}$. This factor was introduced by Albuquerque [4] and can be computed by the following expression:

$$\eta_{TRI} = \frac{(\mathbf{f}-\mathbf{P_0}).\mathbf{d}}{\mathbf{d}.\mathbf{d}} \tag{3}$$

In faces with a skewness factor close to zero, this convective scheme reverts back to the classic one, defined by a distance average since the skewness correction term goes to zero.

The diffusive scheme computes the first derivative of the dependent variable in the normal direction of the face. For the cases with unstructured grids, a scheme with a correction term for the warp angle based on tangential correction (TC) was used, first proposed by Jasak [9]. This correction is required because classic schemes provide a value of the first derivative of $\phi$ in the direction of $\mathbf{d}$, while the desired value is in a direction parallel to the face surface vector $\mathbf{S}_f$. This scheme was shown by Jasak [9] and Magalhães [3] to be superior to other warp angle correction approaches.

$$(\nabla\phi)_f = (\phi_{P_1}-\phi_{P_0})\mathbf{p}_{TC} - \underbrace{\left[(\overline{\nabla\phi})_f - (\mathbf{d}.(\overline{\nabla\phi})_f)\mathbf{p}_{TC}\right]}_{\textbf{warp angle correction}} \tag{4}$$

where the vector $\mathbf{p}_{TC}$ is obtained by decomposing the face surface vector $\mathbf{S}_f$ in two components: one parallel to the distance vector $\mathbf{d}$ and another one tangent to the face itself. This vector can be computed by the following expression:

$$\mathbf{p}_{TC} = \frac{\mathbf{S}_f}{\mathbf{S}_f.\mathbf{d}} \tag{5}$$

To compute the cell centred gradients, the Gauss method is used. This quantity is required for the pressure gradient term and for the correction terms presented, previously. After applying the Gauss method to the volume integral and some mathematical manipulation the following equation is obtained:

$$(\nabla\phi)_P = \frac{1}{V_P}\sum_{f\in\mathcal{F}(P)}\phi_f\,\mathbf{S}_f \tag{6}$$

where the second order assumption inside the cell was considered and the $\phi_f$ value is computed using the previous described convective scheme. Which it self depends of the cell centered gradient information and as a consequence it needs to be solved iteratively, where in the first iteration the skewness correction term is neglected. Normally this procedure convergences in three iterations.

In all unsteady simulations, an Implicit-Euler temporal scheme is used. By considering that the Navier-Stokes equations are written in the following form:

$$\frac{\partial \phi}{\partial t} = F(\phi, t) \tag{7}$$

where $F(\phi, t)$ corresponds to all the terms of the momentum equations except the temporal one. The Implicit-Euler scheme is then defined as:

$$\frac{\phi^{n+1} - \phi^n}{\Delta t} = F(\phi^{n+1}, t^{n+1}) \tag{8}$$

where $\Delta t$ corresponds to the defined time step, $\phi^{n+1}$ and $\phi^n$ are the values on the current and previous time instances, respectively.

## 2 Immersed Boundary Method

The implemented immersed boundary method is based in a conservative cut approach, which retains the shaped of all cells from the original grid and divides it into $n+1$ blocks. One of these blocks, represents the fluid region and the other ones represent the solid regions from the $n$ solid bodies of the problem. The faces that are located between a fluid and a solid block are identified as IB faces and cells inside a fluid region are identified as fluid cells.

After this categorization process, a solid point is computed for each IB face, which is the closet point from the body's surface to the IB face. With the velocity values from the neighbouring solid points and fluid cells of the IB face, a polynomial can be fitted with the least-squares method. Afterwards, a velocity value at the centroid of the IB face is computed, to impose a Dirichlet boundary condition at this location.

During the polynomial fitting of the velocity field, a divergence-free constraint is applied to both polynomials of the velocity components, $u$ and $v$, which are coupled and computed simultaneously (in the same least-squares problem). The divergence-free condition or continuity constraint is defined by:

$$\nabla \cdot \mathbf{u} = 0 \quad \Rightarrow \quad \frac{\partial u}{\partial x} = -\frac{\partial v}{\partial y} \tag{9}$$

This constraint requires that some coefficients of the polynomials are related with each other. Additionally, these polynomials are centred at the main solid point location and have their velocity values $u_s$ and $v_s$ constrained, which are always known since they are equal to the body's velocity. After all mathematical manipulations, the two polynomials of the velocity field have the following form:

$$(u - u_s) = a_1 x + a_2 y + a_3 x^2 + a_4 y^2 + a_5 xy + a_6 x^2 y \tag{10}$$

$$(v - v_s) = b_1 x - a_1 y + b_3 x^2 - \frac{a_5}{2} y^2 - 2a_3 xy - a_6 xy^2 \tag{11}$$

where the some coefficients of the $u$ and $v$ are shared due to the divergence-free constraint. With these, the least-squares matrix is assembled by compiling the polynomials of both velocity components, resulting in:

$$\begin{bmatrix} x_1 & y_1 & x_1^2 & y_1^2 & x_1 y_1 & x_1^2 y_1 & 0 & 0 \\ -y_1 & 0 & -2x_1 y_1 & 0 & -y_1^2/2 & -x_1 y_1^2 & x_1 & x_1^2 \\ x_2 & y_2 & x_2^2 & y_2^2 & x_2 y_2 & x_2^2 y_2 & 0 & 0 \\ -y_2 & 0 & -2x_2 y_2 & 0 & -y_2^2/2 & -x_2 y_2^2 & x_2 & x_2^2 \\ & & & & \vdots & & & \\ x_n & y_n & x_n^2 & y_n^2 & x_n y_n & x_n^2 y_n & 0 & 0 \\ -y_n & 0 & -2x_n y_n & 0 & -y_n^2/2 & -x_n y_n^2 & x_n & x_n^2 \end{bmatrix} \begin{bmatrix} a_1 \\ a_2 \\ a_3 \\ a_4 \\ a_5 \\ a_6 \\ b_1 \\ b_3 \end{bmatrix} = \begin{bmatrix} u_1 - u_s \\ v_1 - v_s \\ u_2 - u_s \\ v_2 - v_s \\ \vdots \\ u_n - u_s \\ v_n - v_s \end{bmatrix} \tag{12}$$

where $n$ is the number of points in the stencil. Note that in this matrix, each two consecutive rows correspond to a single stencil point, with one row for each velocity component.

The following method enforces a divergence-free interpolation and it was proved that suppress the known issue of the spurious forces oscillations (SFO). More details of the current method are explained in the work of Martins *et al.* [7].

## 3 RESULTS

### 3.1 Method Verification with the 2D Analytical Cavity Problem

The analytical solution of the 2D lid-driven cavity is used to study the numerical error of the interpolation method. The problem consists of a square cavity with rigid wall boundary conditions for all boundaries except in the upper one, where the analytical velocity is imposed. This test case was chosen because an analytical solution to the incompressible Navier-Stokes equations is known and it was used by several authors [10–12]. The velocity prescribed on the upper boundary is equal to:

$$u(x, 1) = 16\zeta_1(x) \tag{13}$$

$$v(x, 1) = 0 \tag{14}$$

and the following source term $\beta$ must be added to the vertical momentum equation:

$$\begin{aligned} \beta(x, y) = \frac{8}{Re} \left[ 24 \int \zeta_1(x) dx + 2\zeta_1'(x)\zeta_2''(y) + \zeta_1'''(x)\zeta_2(y) \right] \\ -64 \left[ \Phi_2(x)\Psi(y) - \zeta_2(y)\zeta_2'(y)\Phi_1(x) \right] \end{aligned} \tag{15}$$

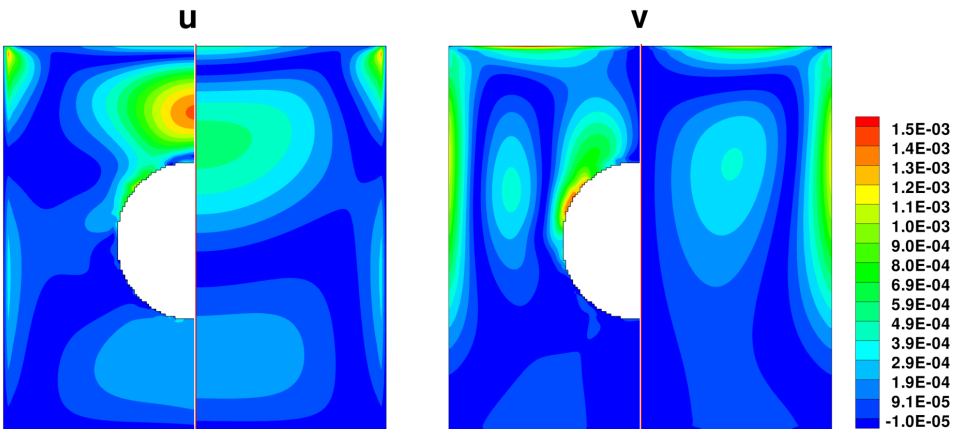


**Figure 2**: Error distribution of the two velocity components for the analytical cavity case with (left) and without (right) the immersed cylinder body.

where $'$ is the differential operator and the functions $\zeta_1(x)$, $\zeta_2(y)$, $\Phi_1(x)$, $\Phi_2(x)$ and $\Psi(y)$ are defined by:

$$\zeta_1(x) = x^4 - 2x^3 + x^2 \tag{16}$$

$$\zeta_2(y) = y^4 - y^2 \tag{17}$$

$$\Phi_1(x) = \zeta_1(x)\zeta_1''(x) - \zeta_1'(x)\zeta_1'(x) \tag{18}$$

$$\Phi_2(x) = \int \zeta_1(x)\zeta_1'(x)dx \tag{19}$$

$$\Psi(y) = \zeta_2(y)\zeta_2'''(y) - \zeta_2'(y)\zeta_2''(y) \tag{20}$$

The domain consists of a $1 \times 1$ box and the chosen Reynolds number was 1 in order to give similar weight to both convective and diffusive terms.

The analytical solution of this problem is:

$$u(x, y) = 8\zeta_1(x)\zeta_2'(y) \tag{21}$$

$$v(x, y) = -8\zeta_1'(x)\zeta_2(y) \tag{22}$$

To demonstrate the accuracy of the immersed boundary method, a cylinder with a radius of 0.2 is introduced in the center of the domain. In this cylinder's *solid points*, the analytical values for $u$ and $v$ are imposed, in the same way they would be imposed for the case of a moving body. Afterwards, the least-squares interpolation uses information of the solid points and neighbouring fluid cells to compute the velocities at the IB faces.

Figure 2 shows the error distribution of both velocity components obtained with and without the immersed cylinder. It can be concluded that the interpolation of the immersed boundary method does not introduced any significant error in the fluid region.

The main difference when using the IB method with a Cartesian grid versus an unstructured one is the conservative cut performed and the least-squares stencil. In figure 3, three different grids are shown with the resulting conservative cuts around a heart-shape geometry. It can be observed that the obtained cut varies wildly with the considered grid

type. It also affects the distance between the immersed boundary and the solid surface, and therefore the interpolation polynomial's domain.

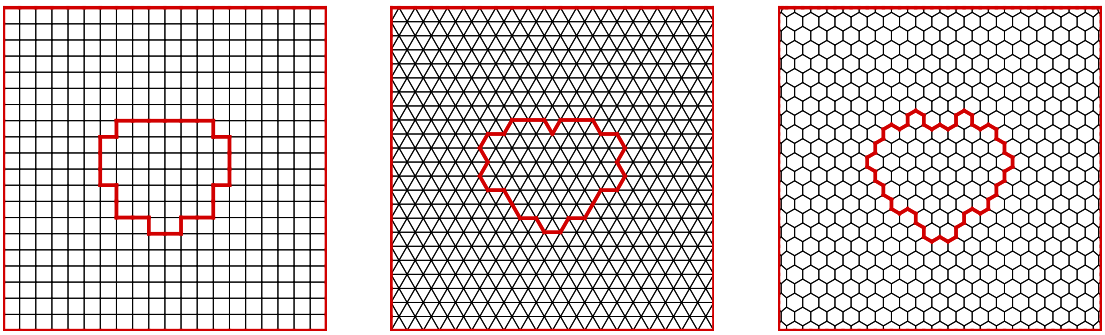

**Figure 3**: Examples of the conservative cut for a Cartesian, triangular and polyhedral grids.

Figure 4 shows the error distribution of the method for a triangle and a polyhedral grid, where once again, the maximum error detaches from the immersed boundary. This observation validates the method as an accurate and robust one, which produces good results independently of grid topology and the considered body geometry.

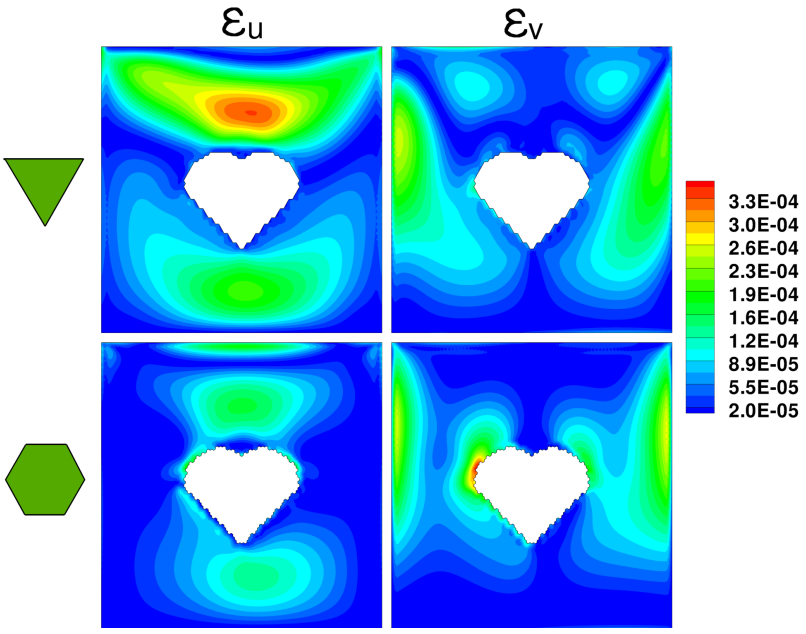


**Figure 4**: Error distribution of the velocity components for a triangular and polyhedral grid.

### 3.2 2D Flapping Wing - Dragonfly Hovering Flight

The flow over a flapping wing is simulated to test the robustness of the proposed CCLS method in the case of a moving body. This case was first introduced by Wang [13] and it has been extensively studied by Kim and Choi [14], and Albuquerque *et al.* [15]. It has also been commonly used in IB methods works [16–18].

This test case consists in a 2D elliptical wing, moving with a sinusoidal velocity along a line with an angle $\theta_p$ relative to the horizontal axis, while simultaneously rotating around its geometric center. Figure 5 represents a schematic of this wing's movement. The wing's position and pitch angle of this movement can be defined by the following equations:

$$x(t) = \frac{A_m}{2} cos(2\pi f t)\, cos(\theta_p) \tag{23}$$

$$y(t) = \frac{A_m}{2} cos(2\pi f t)\, sin(\theta_p) \tag{24}$$

$$\theta(t) = \frac{\pi}{4} sin(2\pi f t) + \theta_0 \tag{25}$$

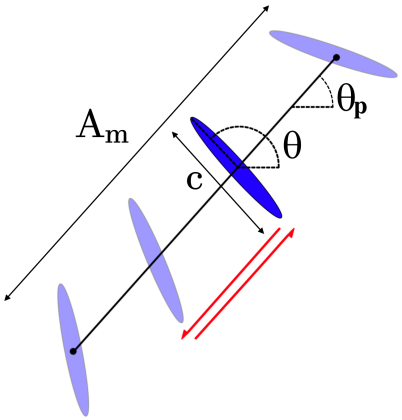


**Figure 5**: Geometric diagram of the flapping wing motion different parameters.

In this variation of the movement: $\theta_p = 60°$, $A_m = 2.5c$, $f = 40\,Hz$ and $\theta_0 = -\pi/4$. The wing consists of an ellipse with a thickness ratio of 8. The Reynolds number is equal to 157, which is based on the maximum translational velocity of the airfoil.

This test case was simulated on a grid of $20c \times 20c$, with a $400 \times 400$ non-uniform grid. In the finest region, which encompasses all body's movement, the grid spacing is $\Delta x = c/80$. A time step of $\Delta t = T/800$ is used, which results in a body Courant number of 0.79 based on the maximum translational velocity. In all outer boundaries, a pressure outlet condition is imposed.

Figure 6 shows the comparison between the horizontal and vertical forces, $CH$ and $CV$, obtained with the proposed method and the ones presented by other works [13–15]. The present calculations show a good agreement with those respective works. Notice that there is a slight disagreement between each work from the literature due to the different used numerical approaches.

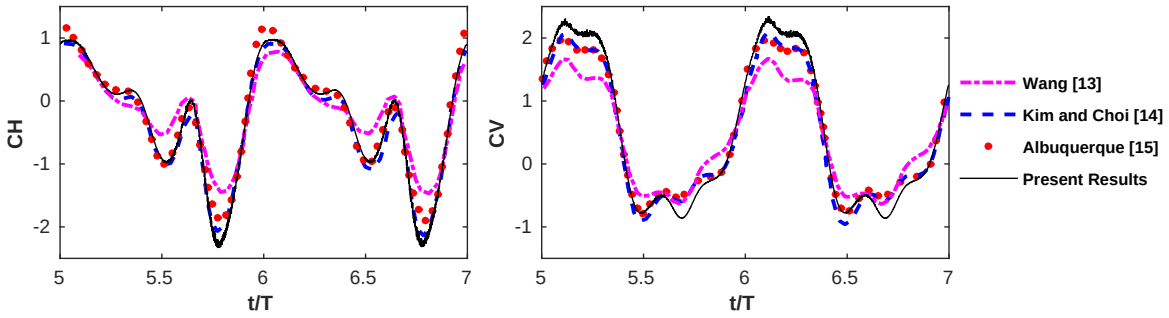


**Figure 6**: Horizontal and vertical force coefficients for the dragonfly hovering flight problem.

### 3.3 2D Flapping Wing - Horizontal Flight

Another flow case was simulated to further demonstrate the capabilities of the proposed CCLS method, which corresponds to a flapping wing in horizontal movement. Which is defined by the following constants $\theta_p = 0°$, $A_m = 2.8c$, $f = 0.25\,Hz$ and $\theta_0 = \pi/2$, corresponding to a Reynolds number of 75. It uses a 2D airfoil with a elliptical form and a thickness ratio of 10.

This test case corresponds to the one studied by Eldredge in [19]. Once again a domain of $20c \times 20c$ with pressure outlet in all outer boundaries is used. The grid contains $400 \times 400$ non-uniformly distributed cells, with $\Delta x = c/160$ in the finest region. The time step is $\Delta t = T/800$, which results in a maximum body Courant number of 0.88.

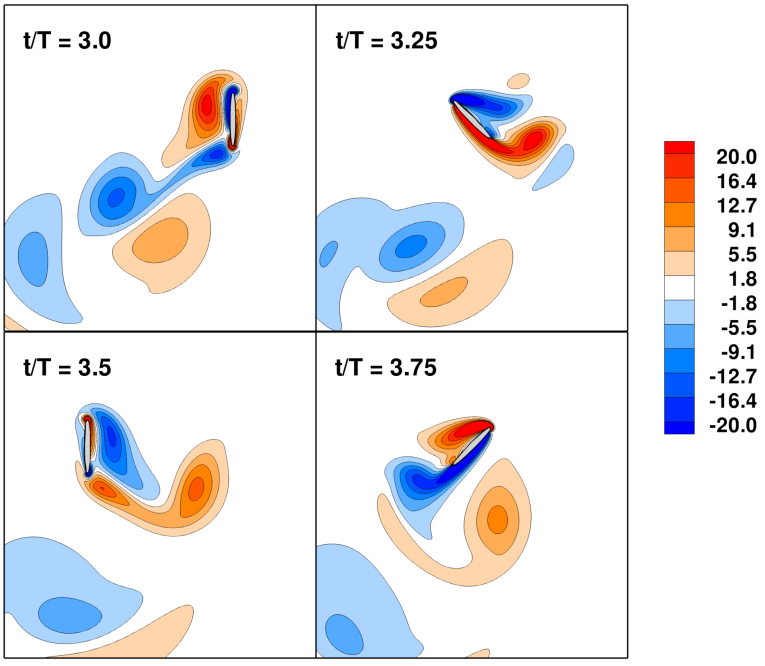


**Figure 7**: Instantaneous vorticity contours for the horizontal flight problem.

Figure 7 shows the instantaneous vorticity contours at four instants of the movement. The vorticity was nondimensionalized by the wing chord and the maximum body velocity. An excellent agreement is observable with the results presented by Eldredge [19].

## 4 CONCLUSIONS

- The extension to unstructured polyhedral grids of the divergence-free interpolation for the immersed boundary methods is described in this work. It is based in a conservative cell cut which has the advantage of not affecting the local grid quality due to the presence of the immersed solid body. The least-squares method used during the interpolation process has the required flexibility to be applied in any type of grid topology.

- The results were divided into two parts. In the first one, the accuracy of the method is studied for a static problem with a known analytical solution. The second part consists in cases with a moving body to show that the proposed CCLS method can produce force curves without any type of spurious oscillations and are in agreement with the results obtained in the literature.

## REFERENCES

[1] João P. P. Magalhães, Duarte M. S. Albuquerque, José M. C. Pereira, and José C. F. Pereira. Adaptive mesh finite-volume calculation of 2D lid-cavity corner vortices. *Journal of Computational Physics*, 243:365–381, 2013.

[2] Duarte M. S. Albuquerque, José M. C. Pereira, and José C. F. Pereira. Residual least-squares error estimate for unstructured h-adaptive meshes. *Numerical Heat Transfer, Part B: Fundamentals*, 67(3):187–210, 2015.

[3] João P. P. Magalhães. An adaptive framework for the numerical simulation of environmental flows in complex geometries. *PhD Thesis, Instituto Superior Técnico, Universidade Técnica de Lisboa*, 2011.

[4] Duarte M. S. Albuquerque. Numerical computation of incompressible flows on adaptive and unstructured grids. *PhD Thesis, Instituto Superior Técnico, Universidade Técnica de Lisboa*, 2013.

[5] Suhas V. Patankar and D. Brian Spalding. A calculation procedure for heat, mass and momentum transfer in three-dimensional parabolic flows. *International Journal of Heat and Mass Transfer*, 15(10):1787–1806, 1972.

[6] Raad I. Issa. Solution of the implicitly discretised fluid flow equations by operator-splitting. *Journal of Computational Physics*, 62(1):40–65, 1986.

[7] Diogo M. C. Martins, Duarte M. S. Albuquerque, and José C. F. Pereira. Continuity constrained least-squares interpolation for SFO suppression in immersed boundary methods. *Journal of Computational Physics*, 336:608 – 626, 2017.

[8] F. Juretić and A. D. Gosman. Error analysis of the finite-volume method with respect to mesh type. *Numerical Heat Transfer, Part B: Fundamentals*, 57(6):414–439, 2010.

[9] H. Jasak. *Error analysis and estimation in the Finite Volume method with applications to fluid flows*. PhD thesis, Imperial College, 1996.

[10] T. Shih, C. Tan, and B. Hwang. Effects of grid staggering on numerical schemes. *International Journal for Numerical Methods in Fluids*, 9(2):193–212, 1989.

[11] M. Kobayashi, José M. C. Pereira, and José C. F. Pereira. A conservative Finite-Volume second-order accurate projection method on hybrid unstructured grids. *Journal of Computational Physics*, 150:40–75, 1999.

[12] José M. C. Pereira, M. Kobayashi, and José C. F. Pereira. A Fourth-Order-Accurate finite volume compact method for the incompressible Navier-Stokes solutions. *Journal of Computational Physics*, 167:217–243, 2001.

[13] Z. Jane Wang. Two dimensional mechanism for insect hovering. *Physical Review Letters*, 85(10):2216, 2000.

[14] Dokyun Kim and Haecheon Choi. Two-dimensional mechanism of hovering flight by single flapping wing. *Journal of Mechanical Science and Technology*, 21(1):207–221, 2007.

[15] Duarte M. S. Albuquerque, José M. C. Pereira, and José C. F. Pereira. Calculation of a deformable membrane airfoil in hovering flight. *Computer Modeling in Engineering & Sciences(CMES)*, 72(4):337–366, 2011.

[16] Jongho Lee, Jungwoo Kim, Haecheon Choi, and Kyung-Soo Yang. Sources of spurious force oscillations from an immersed boundary method for moving-body problems. *Journal of Computational Physics*, 230(7):2677–2695, 2011.

[17] Haoxiang Luo, Hu Dai, Paulo J. S. A. Ferreira de Sousa, and Bo Yin. On the numerical oscillation of the direct-forcing immersed-boundary method for moving boundaries. *Computers & Fluids*, 56:61–76, 2012.

[18] Jinmo Lee and Donghyun You. An implicit ghost-cell immersed boundary method for simulations of moving body problems with control of spurious force oscillations. *Journal of Computational Physics*, 233:295–314, 2013.

[19] Jeff D. Eldredge. Numerical simulation of the fluid dynamics of 2D rigid body motion with the vortex particle method. *Journal of Computational Physics*, 221(2):626–648, 2007.